JET-P(95)46

Physics Issues of ECE and ECA for ITER

D V Bartlett
and members of the
European Home Team for Microwave Diagnostics

JET Joint Undertaking, Abingdon, Oxfordshire, OX14 3EA, UK.

Preprint of a Paper to be submitted for publication in
the proceedings of the International Workshop on Diagnostics for ITER,
Varenna, Italy, 28 August–1 September 1995

September 1995

PHYSICS ISSUES OF ECE AND ECA FOR ITER

D V Bartlett

JET Joint Undertaking, Abingdon Oxon, OX14 3EA, UK

and members of the European Home Team for Microwave Diagnostics *

ABSTRACT

The parameters predicted for the core of ITER plasmas are sufficiently different to those of existing tokamaks that a re-evaluation of the physics basis of ECE measurements is required. This is particularly important in the light of the detailed, and demanding, targets for the measurement of these parameters which have been set in the ITER design. In this paper we examine quantitatively the localisation of ECE T_e measurements in the core and edge plasma, as well as the problem of access to the plasma centre at high T_e. It is concluded that while ECE will be able to provide good measurements of T_e for a wide variety of plasma conditions, the limitations need to be analysed in detail. We also look briefly into the possible potential of ECA as a divertor plasma diagnostic.

INTRODUCTION

The physics issues addressed in this paper are those concerned with the localisation of T_e measurements and the access for those measurements to the plasma centre, since these are the most likely areas of change from the ECE T_e measurements on current tokamaks. The applications of ECE measurements and other ECE physics related issues, such as the consequences of emission from current drive electrons, or the need for an accurate knowledge of the plasma internal magnetic fields, are not discussed here. The experimental issues are considered in another paper [1] at this workshop.

The most important factor determining the behaviour of the core plasma Electron Cyclotron Emission (ECE) in ITER will be the high electron temperatures (>20 keV). Also significant will be the small aspect ratio (which causes harmonic overlap and so limits access to the plasma centre) and the possibility of high electron densities (which might limit access for low frequencies). The large plasma volume (which increases the emission in the high frequency, optically thin, region) will influence the overall form of the emission spectrum. A preliminary investigation of these effects was made during the ITER CDA [2]. In the present work, the consequences of these effects have been evaluated by running a

number of ECE simulation codes for realistic ITER parameters and measurement scenarios. This allows the accessibility (limited by re-absorption in other harmonics) and the spatial resolution (set by spectral broadening) to be determined.

Edge T_e measurements have the same physical basis as the core measurements, but the different plasma conditions (particularly the strong gradients of density and temperature) result in different behaviour for the spatial resolution. This is discussed in relation to the demanding spatial resolution requirements set by ITER

Electron Cyclotron Absorption (ECA) may be able to provide useful Te related information over a reasonably wide range of divertor plasma parameters. The accessible parameter range will be described and the possible performance of a measurement system, based mainly on extrapolation of present experiments, will be discussed.

The paper begins by recalling briefly the method by which ECE spectra are simulated. An example spectrum for predicted ITER conditions is shown. A qualitative explanation of the behaviour of ECE at high T_e is used to explain the features of this spectrum and to illustrate the problem of access to the plasma centre and localisation of the measurements in the core and edge plasmas. The possibility of reducing harmonic overlap by using near vertical sightlines through the plasma is discussed. Quantitative results from the simulations are compared with the requirements for T_e measurements which have been established as part of the ITER design. Finally, the physics basis and likely performance of a divertor ECA diagnostic are discussed.

SIMULATION METHOD AND PLASMA PARAMETERS

In this paper we are concerned with emission from a Maxwellian plasma, and the following simple analysis is appropriate. For each radiation frequency of interest it is necessary to solve the radiation transport equation [3]:

$$dT_{RAD}(s)/ds = j(s) - T_{RAD}(s).\alpha(s)\,, \tag{1}$$

where s is a variable describing the distance along the ray path through the plasma, the radiation intensity is represented as radiation temperature T_{RAD} (defined as the temperature of a black-body which would radiate the same power at the given frequency) and j and α are the emission and absorption coefficients respectively. In a Maxwellian plasma we can use Kirchhoff's law to replace $j(s)$ by $\alpha(s)$ and the electron temperature:

$$dT_{RAD}(s)/ds = \alpha(s).\left(T_e(s) - T_{RAD}(s)\right). \tag{2}$$

This equation has this solution for the intensity emerging from the plasma:

$$T_{RAD} = T_O.e^{-\tau} + \int_{IN}^{OUT} G(s).ds\,, \tag{3}$$

where $T_O.e^{-\tau}$ represents the intensity of the radiation entering the plasma by wall reflections and attenuated by the total optical depth:

$$\tau = \int_{IN}^{OUT} \alpha(s).ds\,. \tag{4}$$

The integrations in Equations 3 and 4 are carried out along the ray path, from where it enters to where it leaves the plasma. The integrand in Equation 3 is

$$G(s) = T_e(s).\alpha(s).e^{-\tau(s)}\,, \tag{5}$$

where $\tau(s)$ is the cumulative optical depth:

$$\tau(s) = \int_{s}^{OUT} \alpha(s').ds \ . \qquad (6)$$

In the present case, we are interested in local temperature measurements so we restrict the discussion to those frequencies for which the total optical depth of the plasma is large, that is, $e^{-\tau} = 0$. This means that T_O is not important and the localisation of the observed emission is determined entirely by the spatial width of the function $G(s)$.

There is a large body of theory in the literature concerned with electron cyclotron interactions in tokamak plasmas (see for example [4] and [5]), and a wide variety of approximations, appropriate to the calculation of emission and absorption coefficients in different circumstances are available.

Also, a large number of ECE simulation codes exists, each code either specifically including or excluding various physics ingredients, and using a variety of techniques to obtain the absorption coefficient. The initial feasibility study for ITER by the European Home Team [6] included a quantitative comparison of six of the codes available in European laboratories. While some differences between the codes were apparent, the level of agreement is certainly good enough to give confidence that predictions made for conditions within the limits of validity of each code are reliable. Most of the results presented here are from the JET code which uses a formulation of the absorption coefficient due to Bornatici [5], which is valid for propagation perpendicular to the magnetic field, high electron temperatures, and includes the "finite density" effects. The limitation to perpendicular propagation is not a problem for the illustrative results presented here, but more general calculations, valid for arbitrary directions, will be needed to complete this study.

Figure 1 shows some results from the JET code which illustrate the behaviour of the quantities $\alpha(s)$, $\tau(s)$, $G(s)$ and the cumulative integral of $G(s)$ for the second harmonic extraordinary mode (E-mode) with ITER-like plasma parameters. The cumulative integral of $G(s)$ is defined in the same way as that for the optical depth (Equation 6), and for convenience we denote it by $\int G(s)$. The shape of the $\alpha(s)$ curve arises from the relativistic expression for the cyclotron resonance frequency, for propagation perpendicular to $\underline{B}$ (ie without Doppler broadening):

$$\omega = m.\frac{e.B}{m_e}, \qquad (7)$$

where m is the harmonic number (m=2 in Figure 1), e is the electron charge and m_e is the relativistic electron mass. The width of $\alpha(s)$ is due to the Maxwellian distribution function giving rise to a range of electron masses, the higher masses requiring a stronger magnetic field (ie. smaller R) to radiate at the given frequency. The vertical line on each plot of Figure 1 is at the location of the non-relativistic cyclotron resonance, obtained by substituting the electron rest mass, m_O, in Equation 7.

A significant feature of Figure 1 is that although the absorption coefficient profile is very wide (> 2m), the width of $G(s)$ is only about 0.1m. This is because the optical depth is large and there is almost total re-absorption of radiation emitted over most of the line width. For observations from the outboard side, only the outer surface of the resonance layer is seen. To quantify the spatial localisation of the observed emission, we use the fact that, according to Equation 3, $\int G(s)$ determines the intensity reaching a measurement antenna. We therefore use the three levels marked on the $\int G(s)$ curve: 90% of the observed intensity originates from the region between the 5% and 95% points, while the 50% point may be considered as the mean radius from which the observed emission originates.

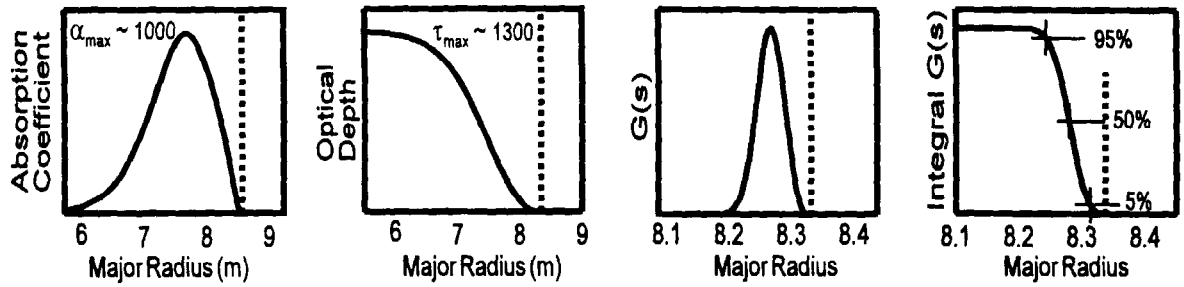

Figure 1: From left to right the curves are: the absorption coefficient for the second harmonic E-mode for typical ITER conditions, the optical depth obtained by integrating the absorption coefficient (Eq. 6), the function *G(s)* (Eq. 5) and its cumulative integral. The radii corresponding to the levels marked on the $\int G(s)$ curve are used to characterise the localisation of the emission (see text).

ITER PLASMA PARAMETERS AND AN EXAMPLE ECE SPECTRUM

To date, two sets of plasma parameters provided by ITER [7] have been used in the simulations. These parameters have been derived from transport code simulations of ITER reference ELMy H-mode conditions. They exhibit the typically flat density profile of H-modes. One set (denoted "CASE1") simulates a sawtoothing discharge and has a flat region at the centre of the T_e profile, while the other ("CASE2") is sawtooth free and has a peaked T_e profile. The full magnetic equilibrium of these discharges is used in the ECE simulations. Figure 2 shows the n_e and T_e profiles for these two cases. The flux surfaces for CASE1 can be seen in figure 7.

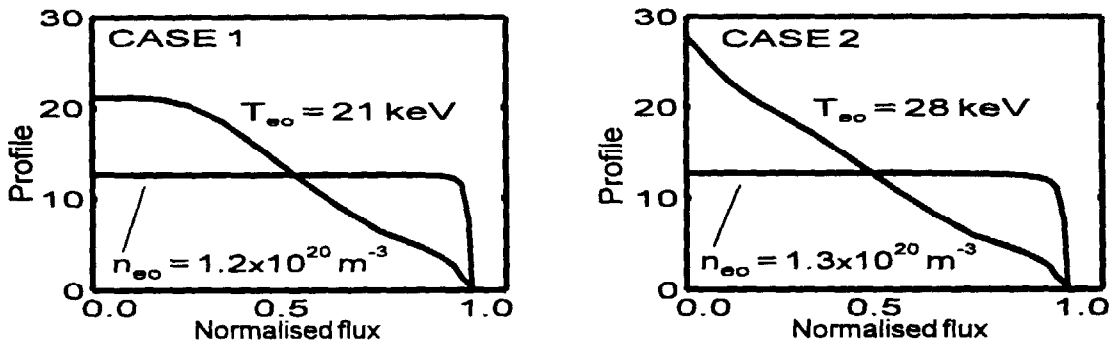

Figure 2: ITER density and temperature profiles used in the ECE simulations. The sawtoothing discharge on the left is referred to as CASE1, while the sawtooth free plasma on the right is denoted CASE2.

Figure 3a shows an example of an E-mode ECE spectrum calculated for CASE1 conditions, using the method described above. A simple model of wall reflections has been included, but this affects only the very low and very high frequency regions. The spectrum appears to consist of the usual series of overlapping harmonics, from which it should be possible to obtain localised measurements of the electron temperature profile. Using the second harmonic region of the spectrum and the $|\underline{B}|$ profile shown in Figure3b, the usual, simple, analysis which uses the non-relativistic resonance condition (Equation 7 with $m_e = m_o$), gives the result shown in Figure 3c. There appear to be three problems in this deduced T_e profile: excess harmonic overlap (in a region where the geometry of the magnetic field indicates that overlap should not occur), an outward shift of the deduced profile on the outboard side, and an overestimate of T_e in the edge region.

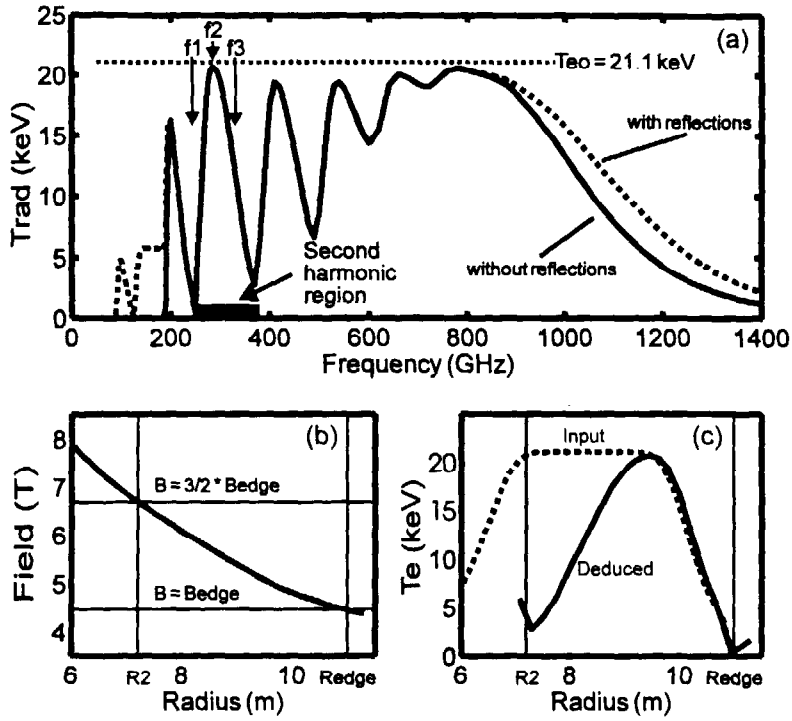

Figure 3: Part (a) is an example of a simulated extraordinary mode ECE spectrum, both with and without wall reflections. The frequencies labelled f1, f2 and f3 are referred to in Figure 4. Part (b) shows the spatial profile of |B| used in the simulation, and used to deduce a T_e profile from the second harmonic region of the spectrum. The radius and field at which third harmonic at the outer edge starts to overlap the second harmonic is indicated. The deduced profile, in part (c), is obtained using the non-relativistic resonance condition. It shows some differences compared to the profile which was used as input to the calculations.

A qualitative understanding of the behaviour of the deduced temperature profile in Figure 3 can be obtained from the sketches of the absorption coefficient in Figure 4. Frequency f_1 corresponds to second harmonic E-mode emission from close to the plasma edge: unless the edge optical depth is large, the tail of $\alpha(s)$ (which is in a region of much higher temperature) can dominate the observed intensity. At frequency f_2 the second harmonic has large optical depth and a well localised value of T_e is obtained. At even higher frequencies, f_3, the tail of $\alpha(s)$ due to the third harmonic enters the plasma (even though the non-relativistic resonance of the third harmonic may be well outside it) and begins to obscure the second harmonic emission.

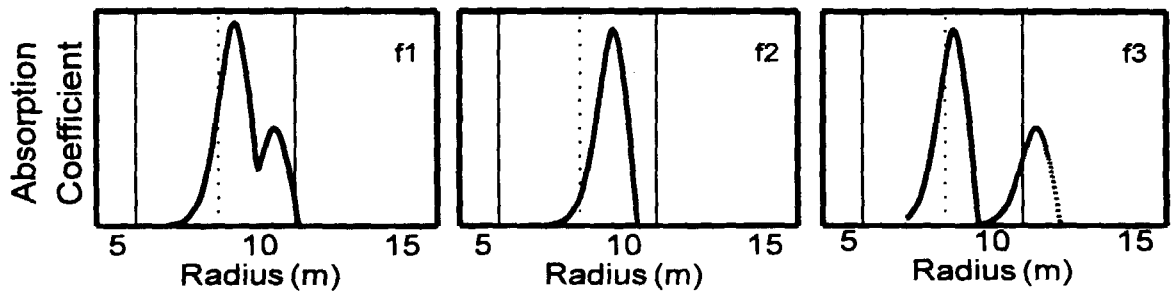

Figure 4:.Sketches of the absorption coefficient for the three frequencies around the second harmonic region which are indicated on Figure 3. The solid vertical lines mark the inner and outer edges of the plasma.

LOCALISATION AND ACCESS TO THE PLASMA CENTRE

From the above discussion it is clear that it is not possible to obtain information about the localisation of the emission simply by looking at spectra, such as the one shown in Figure 3 . A better way to present this information is to plot the location and width of the function $G(s)$ as a function of frequency, on a graph of frequency vs. radius. Examples are shown in Figure 5, for both the E-mode and the ordinary mode (O-mode), for an antenna on the outboard side on the plasma midplane, and for the plasma conditions of CASE1. The horizontal bars link the radii corresponding to the 95% and 5% levels of $\int G(s)$, while the

thicker central line marks the 50% level. At each frequency, the intensity which would be measured is the average of T_e across the radial width of the bar. These bars and the central line are drawn over the frequency range for which the plasma is optically thick. This range is indicated by the vertical bar next to the frequency scale. Also shown are the locations of the non-relativistic cyclotron resonances (Equation 7 with $m_e = m_0$, and using the spatial variation of $|\underline{B}|$ given by the equilibrium data), and the cutoff locations for each polarisation mode.

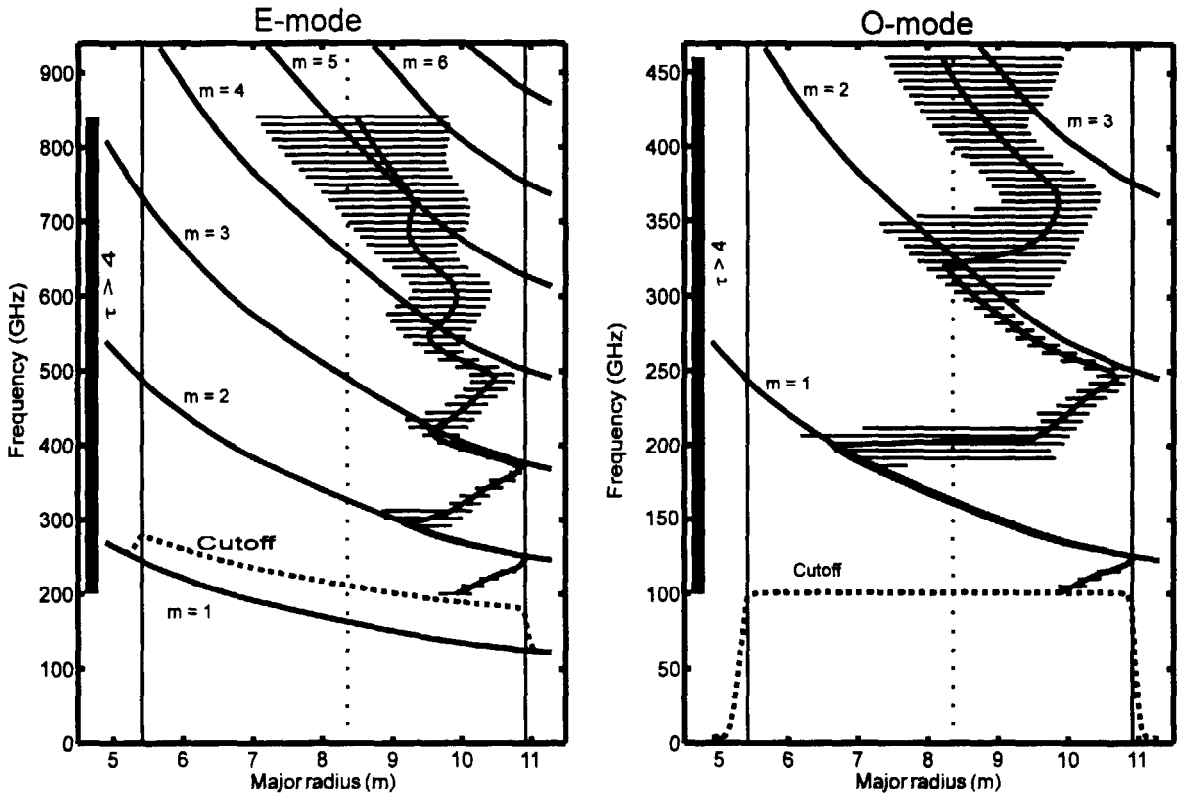

Figure 5: Horizontal bars representing the width and location of the emitting layer on a frequency vs. radius plot. The intensity which would be measured at each frequency by an outboard side antenna on the plasma midplane is the average temperature across the bar. The left hand plot is for the E-mode, and the O-mode is on the right. In each case the non-relativistic cyclotron harmonics are shown as well as the appropriate cutoff locations. The vertical bar next to the frequency axis shows the frequency range for which the plasma is optically thick.

Using the data in this figure the behaviour of the deduced T_e profile, explained qualitatively in Figure 4, can be made quantitative. Over some part of the second harmonic E-mode (and most of the first harmonic O-mode) the emission is localised to a narrow band just behind the non-relativistic cyclotron harmonic. The inward shift, relative to the non-relativistic resonance, is not a serious problem since its magnitude can be estimated quite accurately from an approximate knowledge of n_e and T_e. At higher frequencies, emission which is downshifted from the next higher harmonic starts to obscure the well localised emission and T_e measurements are not possible. At lower frequencies, close the plasma edge, there is not sufficient optical depth to re-absorb downshifted emission from the same harmonic which is emitted deeper in the plasma. Higher harmonics (third harmonic E-mode and second harmonic O-mode) show some moderately localised emission over a small radius range. For these plasma conditions, there are no frequencies for which there is well localised E-mode emission from near the plasma centre, but localised T_e measurements at radii well inboard of the centre are possible in the O-mode.

Repeating these calculations with either the n_e or T_e profiles multiplied by a scaling factor gives an indication of how the localisation and central access will vary with plasma conditions. For T_{eo} below about 15 keV, access to the plasma centre is possible using the second harmonic E-mode. First harmonic O-mode emission from the plasma centre can propagate to the outboard side for T_{eo} up to about 30 keV and (limited by cutoff) densities up to about 3×10^{20} m^{-3}. Over this parameter range the width of localisation in both polarisation modes does not vary very much. In addition, these conclusions are not strongly affected by changes of density, apart from the problem of cutoff.

NEAR VERTICAL SIGHTLINES TO REDUCE HARMONIC OVERLAP

A possible way of reducing the harmonic overlap, while maintaining propagation almost perpendicular to the magnetic field, is to use near vertical sightlines which are directed towards the plasma centre from a vertical port. The radiation path through the plasma covers a smaller range of radius, and therefore experiences a smaller range of $|\underline{B}|$, which reduces harmonic overlap.

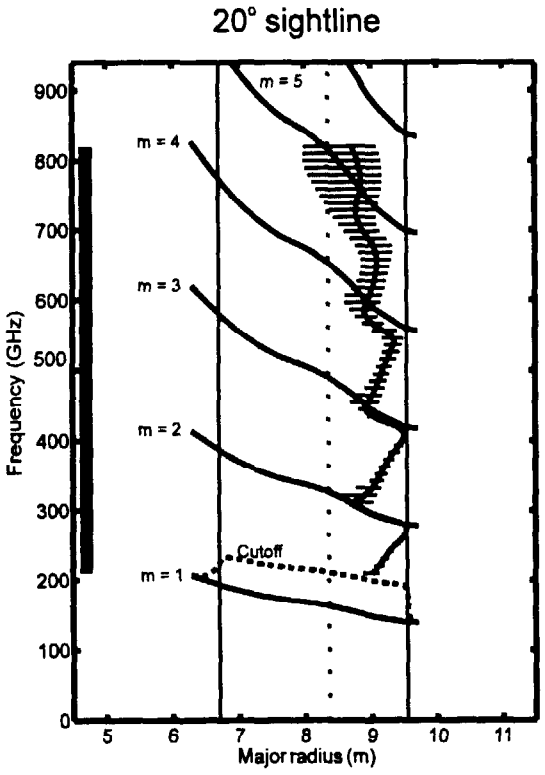

Figure 6: Localisation for the E-mode along a near vertical sightline, showing that the limiting radius in the second harmonic is slightly closer to the plasma centre than for the horizontal sightline of Figure 5.

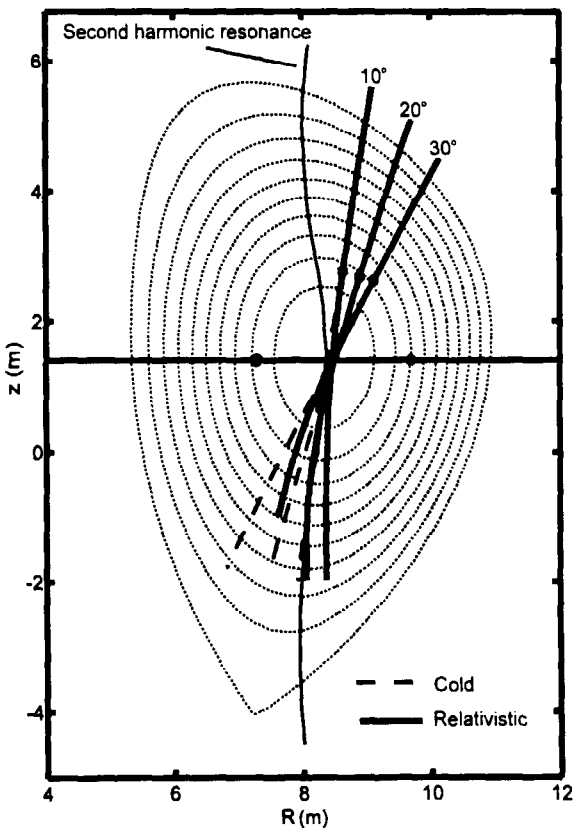

Figure 7: Relativistic ray tracing for the E-mode along three near vertical sightlines. The deflection near the plasma centre is due to anomalous dispersion, and may prevent good access to the centre.

Figure 6 shows the localisation of the second harmonic E-mode for CASE1 plasma conditions, and a sightline 20° from the vertical. Although the overlap in the second harmonic region is reduced compared to the plasma midplane sightline of Figure 5, it is still not possible to reach the centre. Moreover, there is a further effect which becomes important at these high temperatures. Figure 7 is the output from a relativistic ray tracing code [8] for three E-mode rays, launched at angles of 10°, 20° and 30° from the vertical,

PRINCIPLE AND PROJECTED PERFORMANCE OF AN ECA DIAGNOSTIC

It is very unlikely that the plasma conditions in the divertor will be such that a localised measurement of T_e using ECE will be possible. The principle problem is that the magnetic field strength in the divertor region is the same as that in the core plasma, while the electron temperatures should be a factor of 100 or more lower. The intense ECE from the core plasma will reach the divertor region by wall reflections, and a high optical depth ($\tau \sim 8$) in the divertor plasma would be required to attenuate it to a level much less than that of the local emission. The density and temperature predicted for the ITER divertor plasma give optical depth values of order one.

Since the optical depth is too low for useful ECE measurements, the alternative is to determine the optical depth itself by measuring the absorption of radiation from an external source. Such a diagnostic has been constructed for the JET divertor [9]. It must overcome a variety of serious technical difficulties, related to access to the plasma, long waveguides to transport the radiation to and from the divertor, and standing waves which can cause spurious modulation of the transmitted power. Since the experience of the JET system is that these problems can be overcome, we examine here the plasma parameter range over which such a system might be able to operate in the ITER divertor.

The theoretical basis of a calculation is much the same as that presented above for ECE, although simpler in this case, for two reasons. First, we are concerned only with transmission of radiation through the plasma, that is, we obtain the optical depth from an experimentally measured transmission, then use Equation 4 to deduce plasma parameters. Secondly, the spatial width of the absorption coefficient is very small (~ 1 mm) for the low temperatures in the divertor. It can be approximated by a delta function, making the integration in Equation 4 unnecessary. There are, therefore, relatively simple expressions [4] for the spatially localised optical depth as a function of frequency. In the second harmonic E-mode the optical depth is proportional to the density - temperature product. The second harmonic E-mode is the best choice for such a measurement since it has greater optical depth than the first harmonic O-mode and a higher cutoff density.

Taking into account the other ITER parameters, and assuming that transmission can be reliably measured over the range 10% to 90%, the range of $n_e.T_e$ which can be determined is approximately the following for the second harmonic E-mode:

$$2 \times 10^{20}\ \text{eV.m}^{-3} < n_e.T_e < 4 \times 10^{21}\ \text{eV.m}^{-3}. \qquad (8)$$

This equation breaks down at high densities (~ 6×10^{20} m^{-3}), close to cutoff. The result is illustrated graphically in Figure 8, which plots several transmission contours in $n_e.T_e$ space.

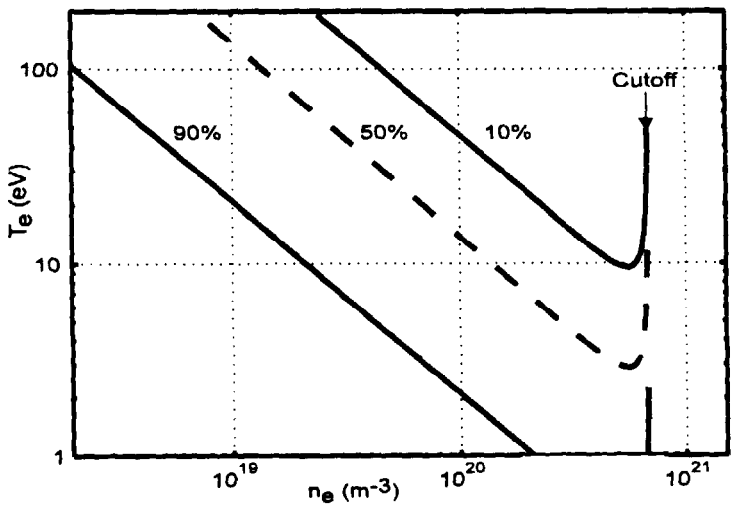

Figure 8: Contours of constant transmission through the ITER divertor plasma in $n_e.T_e$ space, for the second harmonic extraordinary mode. At constant transmission the $n_e.T_e$ product is constant, except near the cutoff.

and calculated for a frequency equal to the central second harmonic. Near the resonance layer, relativistic effects cause anomalous dispersion: a kink in the refractive index whose spatial width increases with T_e. The effect of this perturbation is to deflect the rays which are propagating near vertically away from the resonance layer. This effect is complex to characterise, since both the magnitudes and profiles of n_e and T_e play a role, but it appears that at the high temperatures where harmonic overlap is a problem the deflection will generally be large enough to prevent the plasma centre from being observed.

SUMMARY AND COMPARISON WITH THE ITER REQUIREMENTS

Data of the type plotted in Figure 5 can be used to give a simple summary of the spatial resolution which can be achieved with ECE measurements. Table 1 summarises the results for a horizontal sightline, viewing the plasma from the outboard side and passing through the plasma centre.

Table 1: Spatial resolution of T_e measurements for propagation nearly perpendicular to $\underline{B}$.

	Core plasma, with T_{eo} = 10 keV	Core plasma, with T_{eo} = 20 keV	Plasma edge
First harmonic, O-mode	0.10 m	0.13 m	0.04 - 0.06 m*
Second harmonic, E-mode	0.08 m	0.10 m	0.02 - 0.04 m*

* See note in text.

It is apparent that the ITER target resolution for core plasma measurements of 0.10 m can be achieved. The resolution target of 5 mm set by ITER for edge T_e measurements has not been achieved in these simulations. It should be noted that the edge resolutions given in the table apply to the particular edge profiles used in these calculations. They can only be taken as typical values, since this resolution is strongly profile dependent. For very steep edge T_e profiles the edge resolution is somewhat worse, but it is unlikely that the 5 mm target will be reached for any plasma conditions.

Access to the plasma centre is limited by re-absorption at high temperature (for the second harmonic extraordinary mode) and by cutoff at very high density (for the first harmonic ordinary mode). The results, again for an outboard horizontal antenna with a sightline through the plasma centre, are summarised in Table 2.

Table 2: Access to the plasma centre for T_e measurements.

	Max. T_e for access to centre*	Max. n_e for access to centre*	Inner R limit for CASE1
First harmonic, O-mode	~ 30 keV	~ 3×10^{20} m^{-3}	7.2 m
Second harmonic, E-mode	~ 15 keV	~ 3×10^{20} m^{-3}	9.5 m

* See note in text.

It should be noted that the values for maximum n_e and T_e are dependent on the equilibrium which is used in the calculations: changes in profile shapes would modify the values slightly, while a reduced toroidal field would significantly reduce the density limits.

The only sightlines which might give some improvement in access are those which pass near vertically through the plasma centre. However, the calculations presented here indicate that such improvements are in fact not achieved.

Although the parameter range shown above is wide, it does not cover the whole of the potential range given by current predictions for the ITER divertor (1 to 100 eV and 10^{19} to 10^{22} m^{-3} near the target). A more extensive analysis, including other factors (such as refraction) in the calculations, and using realistic 2-D plasma profiles will be required before more precise predictions can be made.

SUMMARY AND CONCLUSIONS

This paper has shown that the plasma conditions predicted for the core of ITER plasmas are sufficiently different to those of existing tokamaks that the behaviour of electron cyclotron emission is qualitatively different. A re-evaluation of the characteristics of ECE in such plasmas is required. The first stages of this investigation have shown that ECE will be able to provide measurements of electron temperature for a wide variety of plasma conditions. The spatial resolution requirements for such measurements set in the ITER design can be met. There is a problem of access to the plasma centre at high T_e for the second harmonic extraordinary mode, but the this can be overcome by using the first harmonic ordinary mode, except at very high densities.

The potential of ECA as a divertor plasma diagnostic has been examined briefly. A simple theoretical analysis indicates that it should be possible to measure the electron density - electron temperature product over a wide range of the predicted operating space. However, results from current experiments, such as the one at JET, need to be evaluated before reliable predictions, leading to the design of hardware, can be made.

ACKNOWLEDGEMENTS

The author wishes to thank Dr H Bindslev for his considerable efforts in modifying his ray tracing code to operate with the ITER equilibria, and Dr D Boucher for providing the equilibria used in the calculations presented here.

* The members of the European Home Team for Microwave Diagnostics who have participated in this work are: A Airoldi, P Buratti, L Cupido, T Donné, G Giruzzi, H Hartfuss, E Joffrin, M E Manso, S Nowak, R-L Meyer, G Ramponi, J Sanchez, B Schokker, A Silva, P Stott, V Tribaldos, G Waidmann

REFERENCES

[1] H Hartfuss, this workshop.
[2] A E Costley and D V Bartlett, Proc 8th Joint Workshop on ECE and ECRH (Gut Ising, 1993), IPP report IPP III/186.
[3] G Bekefi, "Radiation processes in plasmas", Wiley (1966).
[4] M Bornatici et al, Nuc Fusion **23**, 1153 (1983).
[5] M Bornatici, F Engelmann and U Ruffina, Sov J Quantum Elec, **13**, 68, (1983).
[6] Report by the EU Home Team for ITER Task Agreement S 56 03 94-9-27-F.
[7] D Boucher, private communication.
[8] H Bindslev, Proc 9th Joint Workshop on ECE and ECRH (Borrego Springs, 1995).
[9] R J Smith et al, Proc 8th Joint Workshop on ECE and ECRH (Gut Ising, 1993), IPP report IPP III/186.